Domain wall dynamics in ultrathin Pt/Co/AlOx microstrips under large combined magnetic fields

E. Jué,[1,2,3,*] A. Thiaville,[4,†] S. Pizzini,[5,1] J. Miltat,[4] J. Sampaio,[4] L. D. Buda-Prejbeanu,[1,2,3] S. Rohart,[4] J. Vogel,[5,1] M. Bonfim,[6] O. Boulle,[1,2,3] S. Auffret,[1,2,3] I. M. Miron,[1,2,3] and G. Gaudin[1,2,3]

[1]*Université Grenoble Alpes, 38000 Grenoble, France*
[2]*CEA, INAC, SPINTEC, 38000 Grenoble, France*
[3]*CNRS, SPINTEC, 38000 Grenoble, France*
[4]*Laboratoire de Physique des Solides, Université Paris–Sud, CNRS, UMR 8502, 91405 Orsay, France*
[5]*CNRS, Institut Néel, 38042 Grenoble, France*
[6]*Departamento de Engenharia Elétrica, Universidade Federal do Paraná, Curitiba, Brazil*

(Received 29 October 2014; revised manuscript received 15 October 2015; published 4 January 2016)

The dynamics of magnetic domain walls in ultrathin strip-patterned Pt/Co/AlOx samples with perpendicular easy axis has been studied experimentally under an easy-axis field, superposed to a hard-axis field oriented along the strip. The easy-axis field is large so that the domain walls move well beyond the creep regime. A chiral effect is observed where the domain wall velocity shows a monotonous and surprisingly large variation with an in-plane field. A micromagnetic analysis, combining analytic, one-dimensional, and two-dimensional simulations with structural disorder, shows that this behavior can be reproduced with a Dzyaloshinskii-Moriya interaction of the interfacial type, with due consideration of the dynamics of the tilt degree of freedom of the domain wall. The estimated effective value of this interaction ($D \approx -2.2$ mJ/m^2 for a 0.6 nm Co thickness) is consistent with values obtained by other techniques. It is also shown, by micromagnetic analysis, that several modes and characteristic times occur in the dynamics of the tilt of such domain walls.

DOI: 10.1103/PhysRevB.93.014403

I. INTRODUCTION

Recent studies have revealed that the magnetism of ultrathin films is richer than what is conceived from the mere reduction of film thickness. Indeed, beyond the expected change in the Curie temperature and in thermal fluctuation effects, and beyond the appearance of surface/interface anisotropy and of interfacial exchange coupling, etc., chiral effects have been discovered in such samples. As chirality cannot be defined in a two-dimensional world, and as also shown by experiments, these effects appear when upward- and downward-oriented normals to the film are structurally different (structural inversion asymmetry). The emblematic sample in this respect [1] is an ultrathin cobalt layer with a perpendicular easy axis, capped by aluminum oxide and grown on platinum, a 5*d* metal with large spin-orbit coupling, whereas the capping insulator is made of light elements.

The first observed chiral effect appears to be the switching of the sample's perpendicular magnetization for a unique combination of domain magnetization ($\pm z$), in-plane current ($\pm x$), and in-plane field ($\pm x$) [2,3], where z denotes the film normal and x is an in-plane direction. The second is a chiral change of the velocity of domain walls (DWs) when driven by an in-plane current flowing transverse to the DW, under an in-plane field applied parallel to the current [4,5], wherein for successive DWs, opposite in-plane fields are required to increase the velocity. A closely related effect is a chiral variation of DW energy under an in-plane field applied transverse to the DW, which manifests itself by a chiral change of field-driven velocity in the creep regime [6,7], and by an asymmetric nucleation of reversed domains at the edges of the sample that are normal to the in-plane field [8]. In the first case, the observations have been interpreted by a spin-orbit torque exerted by the in-plane current (in the form of a Rashba effective field [9], or of a spin Hall effect [2,3]). The DW experiments of the second case have been accounted for by the micromagnetic exploration of the dynamics of so-called Dzyaloshinskii domain walls [10], chiral DWs with a (partly or fully) Néel structure, whose stability derives from an interfacial Dzyaloshinskii-Moriya interaction (DMI) [11–14], following the observation of such structures in monolayer and bilayer epitaxial films [15]. These two types of chiral effects are interconnected, because the same forms of spin-orbit torque are invoked when current is applied, and also because magnetization switching in samples extending over more than tens of nanometers occurs via DW nucleation and motion [16]. Thus, the structure and dynamics of DWs in such ultrathin films with perpendicular magnetization and structural inversion asymmetry along the film normal constitute an interesting topic in itself for physics as well as for applications, and also as the basic process of magnetization reversal in these samples.

The simplest and best understood means for acting on a DW is to apply a magnetic field. The field value and time scale fix the regime of DW motion. On the one hand, applying low fields for long times gives access to the creep regime [17], which has been studied in particular in ultrathin films with perpendicular magnetization [17–19] and recently in asymmetric samples [6,7]. In this regime, the DW energy (surface tension) plays a key role, and the intrinsic magnetization dynamics (damped precession around the effective field) is not important. On the other hand, at large fields the flow regime of motion is reached, with the two well-known steady-state and precessional regimes according to the dynamics of the DW moment [20]. For ultrathin films with perpendicular magnetization,

*Present address: NIST, Boulder, CO 80305, USA; emilie.jue.spintec@gmail.com
†andre.thiaville@u-psud.fr

the experimental results for flow reported up to now have evidenced only the precessional regime, be it in samples with symmetrical interfaces such as Pt/Co/Pt [21] or (Co/Ni) [22], or for nonsymmetrical stackings such as Ta/CoFe(B)/MgO [23]. However, as first shown experimentally [9] and interpreted [10] by some of us, in the Pt/Co/AlOx case it seems that the steady-state flow regime is obeyed. The interpretation rests on the stabilization, by interfacial DMI of chiral DWs with an internal magnetization in the Néel orientation. This proposed interpretation requires further tests, which is the object of this paper. We thus investigated DW dynamics in Pt/Co/AlOx under large combined fields, namely an easy-axis driving field together with an in-plane field so as to act on the DW magnetic moment. The work comprises an experimental part (Sec. II), a theoretical part in the frame of micromagnetics (Sec. III), followed by a discussion (Sec. IV) [24].

II. EXPERIMENTS

Experiments were carried out on samples of Pt(3 nm)/Co(0.6 nm)/AlOx(2 nm) deposited on a Si/SiO2 substrate by magnetron sputtering. The Pt/Co/Al metal sample was oxidized *in situ* under an oxygen radiofrequency plasma for 35 s, chosen to optimize the perpendicular magnetic anisotropy (PMA) [25]. The DW dynamics was studied under combined fields: an out-of-plane field H_z (along the easy axis) responsible for the DW displacement, and an in-plane static field H_x (hard axis, normal to the DW) used to tune DW stability. These fields were increased up to observing domain nucleation events.

As a preliminary experiment, we image the influence of an in-plane field on DW displacement for a circular DW (Fig. 1) within an infinite film and in the creep regime in order to compare to existing data [6,7]. The advantage of this configuration is that up/down and down/up DWs can be observed simultaneously in different directions (especially transverse to and along the in-plane field). For this experiment only, since the in-plane field itself cannot drive the DWs, the planar coil used to induce H_x is slightly tilted out-of-plane ($\sim 2^\circ$) in order to apply simultaneously the small z and large x field components. DW motion is probed using a wide-field Kerr microscope. Starting with a circular domain [Figs. 1(a) and 1(b)], DW motion is induced by the application of a 100 mT field during 50 ms along $-x$ and $+x$ directions. Figures 1(c) and 1(d) show differential images of the DW displacement. Dark or bright contrast corresponds, respectively, to an expansion of an up or down domain. We observe that, whereas both up/down and down/up DWs move on a similar distance along the y axis, an asymmetry is observed for the DW displacement along the x axis. It is such that DWs move faster in a counterclockwise (CCW) configuration. Note that the observed asymmetry is opposite to that reported [6] for Pt/Co/Pt.

In the rest of the paper, we study DW motion along one direction only (x, i.e., with DWs normal to the in-plane field). For this, the sample was structured by electron beam lithography and ion beam etching into 2-μm-wide strips. Although DWs inside a stripe are expected to be oriented transverse to the stripe axis, recent studies have shown that a DW tilting can appear in an out-of-plane system with structural inversion asymmetry [26,27]. The width of the stripe has

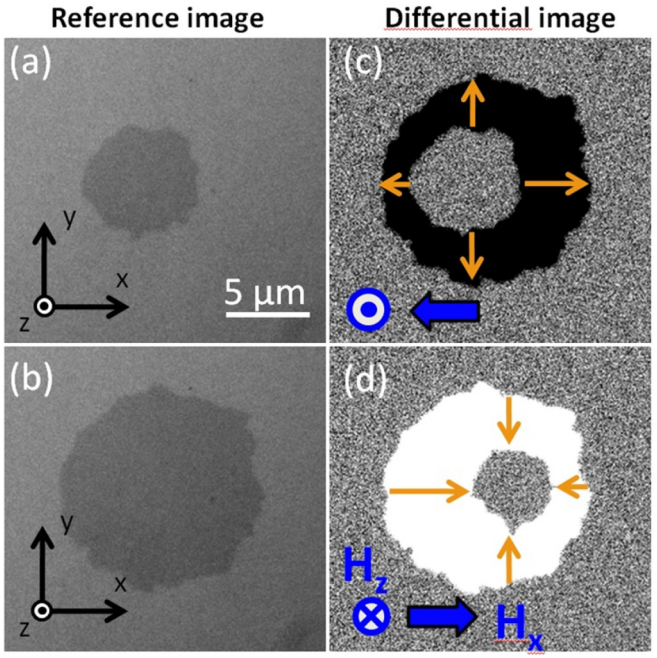

FIG. 1. Displacement of a circular DW under a large H_x slightly tilted out of the plane. (a) and (b) Initial magnetic configuration of the system, with a circular magnetic domain pointing along $+z$ (dark contrast). (c) and (d) Differential image obtained after applying $\mu_0 H_x = \pm 100$ mT with $H_z = -0.035 H_x$ during 50 ms. Orange arrows indicate the direction of DW displacement. An asymmetry of the DW displacement appears along the in-plane field direction. Note that the end configuration in (c) is the starting one for (b).

therefore been chosen large enough to enable optical imaging of such tilts.

With the large out-of-plane driving fields giving rise to large velocities (100 m/s) and increasing the probability of domains nucleation, the field H_z has to be applied with very short pulses (<100 ns). For this, we use a microcoil [28] producing pulses as short as 20 ns for field values ranging from 50 to 200 mT (inset in Fig. 2) that is glued to the sample. For field homogeneity, measurements were taken on the strip closest to the center of the coil. From the optically measured film to microcoil distance, the current to field conversion is estimated to be 6 ± 1 mT/A.

Starting with a saturated sample, two adjacent DWs (one up/down and one down/up) are prepared by nucleating a magnetic domain into the stripe with a first H_z pulse [Fig. 3(a)]. Then, a constant in-plane field is applied along the wire (x axis) and both DWs are moved simultaneously by applying n consecutive pulses of H_z, with a repetition period of 200 ms. DW velocity is determined by dividing the total displacement by the integrated time ($n \times 20$ ns). For statistics, each measurement is repeated several times and the DW displacement is obtained by an average of 40–250 independent events. Finally, in order to avoid misalignment contributions, DW displacement is studied for both up/down and down/up DWs, and for positive and negative fields.

We first investigate DW motion under the sole action of H_z in order to know its mobility regime (Fig. 2). At the

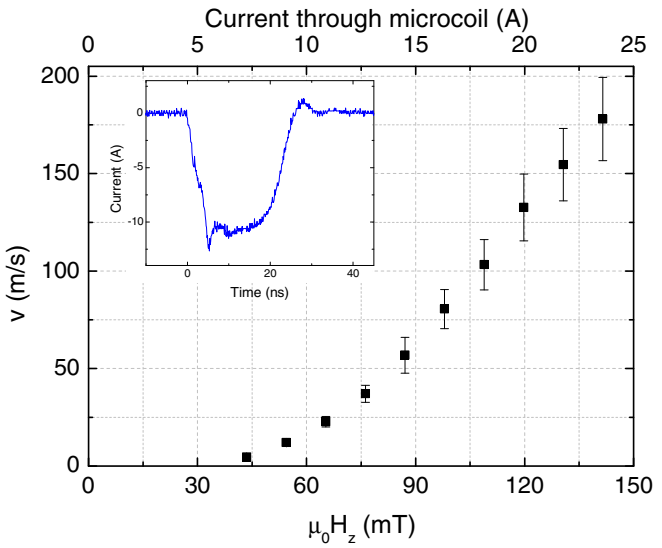

FIG. 2. DW velocity as a function of easy-axis driving field H_z. The inset shows the typical shape of a current pulse through the microcoil with 50 μm inner diameter.

highest field values (≈140 mT), a constant mobility seems to be reached but not with a zero intercept, suggesting that the DW moves in an imperfectly uniform medium (see Appendix A). We note moreover that no discontinuity is observed on the DW velocity versus H_z curve, meaning that no Walker breakdown [10] occurs in the studied field range.

We now focus on the influence of the additional x field on the z field driven DW dynamics. Figure 3(b) shows DW displacements measured with an identical z field in the presence of a static x field varying from -200 to 200 mT. As expected from the preliminary measurements, an asymmetry of DW motion along x appears with the in-plane field, with again a fast DW motion in the CCW configuration. We observe that this asymmetry increases continuously with the magnitude of H_x and depends on both the DW polarity (up/down or down/up) and the sign of H_x. To consider all the symmetries of the system, the measurements were repeated for negative H_z values. The DW velocities for each case are shown in the inset of Fig. 3(c), a positive velocity corresponding to a DW displacement along $+x$. The same behavior is observed in absolute value for both positive and negative H_z, indicating that the asymmetry of the DW dynamics is not affected by the H_z direction but only by H_x. The averaged DW velocity is determined by taking into account both DW polarities and both field directions (mapping all results to the situation of a down/up wall moving under negative H_z):

$$v(H) = \tfrac{1}{4}\{v_{\uparrow\downarrow,+H_z}(-H_x) - v_{\uparrow\downarrow,-H_z}(-H_x) - v_{\downarrow\uparrow,+H_z}(H_x) + v_{\downarrow\uparrow,-H_z}(H_x)\}. \quad (1)$$

The resulting curves [Fig. 3(c)] show a large, monotonous variation of DW velocity with H_x. Note that this variation is not linear: the change of DW velocity is larger for accelerated DWs than for slowed-down DWs.

To study the influence of H_z magnitude on the asymmetry of DW dynamics in the presence of x fields, the measurements

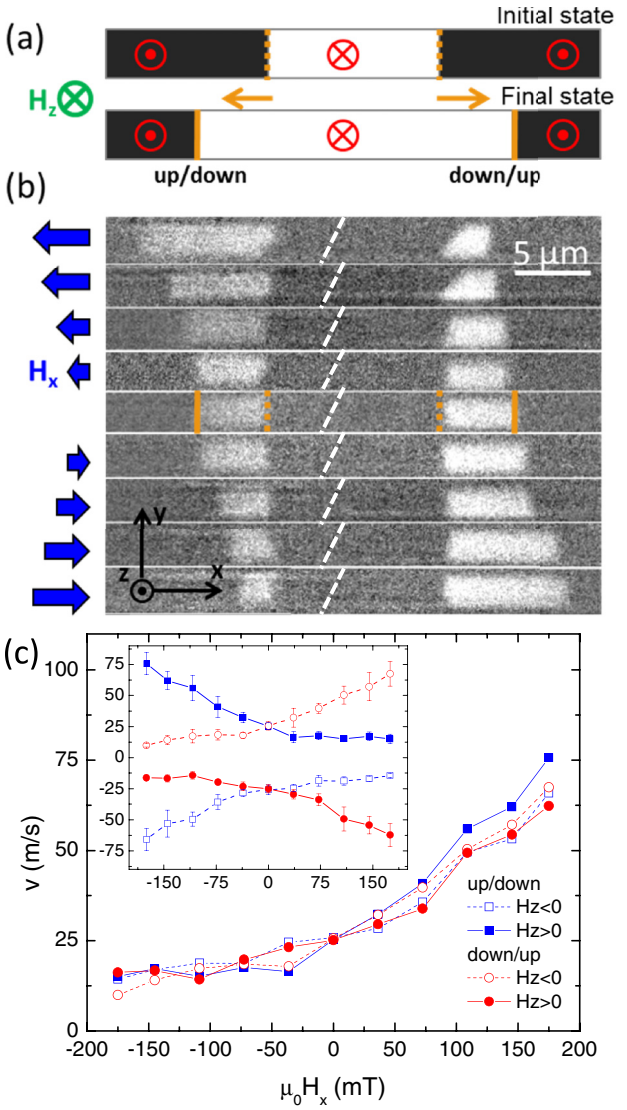

FIG. 3. Influence of the x field on DW motion for a constant z field value. (a) Sketch showing that two adjacent DWs are initially prepared in the center of the wire (dashed lines) and then displaced outward (solid lines) by the driving z field. (b) Differential images of DW displacements. DWs are displaced by seven consecutive pulses of 20 ns and 76 mT in the presence of a static x field varying from -220 to 220 mT (blue arrows). For clarity, images were modified in order to align initial positions of both up/down and down/up DWs (the three tilted initial DWs correspond to stronger pinning positions in the center of the stripe). (c) Average DW velocity obtained by superposition of the four curves shown in the inset after symmetry transformation. Inset: DW velocities as a function of H_x under pulsed $\mu_0 H_z = 64$ mT. Up/down and down/up DW velocities are measured for both directions of fields. The convention is that positive DW velocities correspond to DW displacements along $+x$.

were repeated (on another sample with identical nominal characteristics) for different values of H_z. In this case, measurements are performed for only one direction of H_z (along $-z$), and the averaged velocity is now determined by $v(H) = (1/2)\{v_{\downarrow\uparrow,-H_z}(H_x) - v_{\uparrow\downarrow,-H_z}(-H_x)\}$.

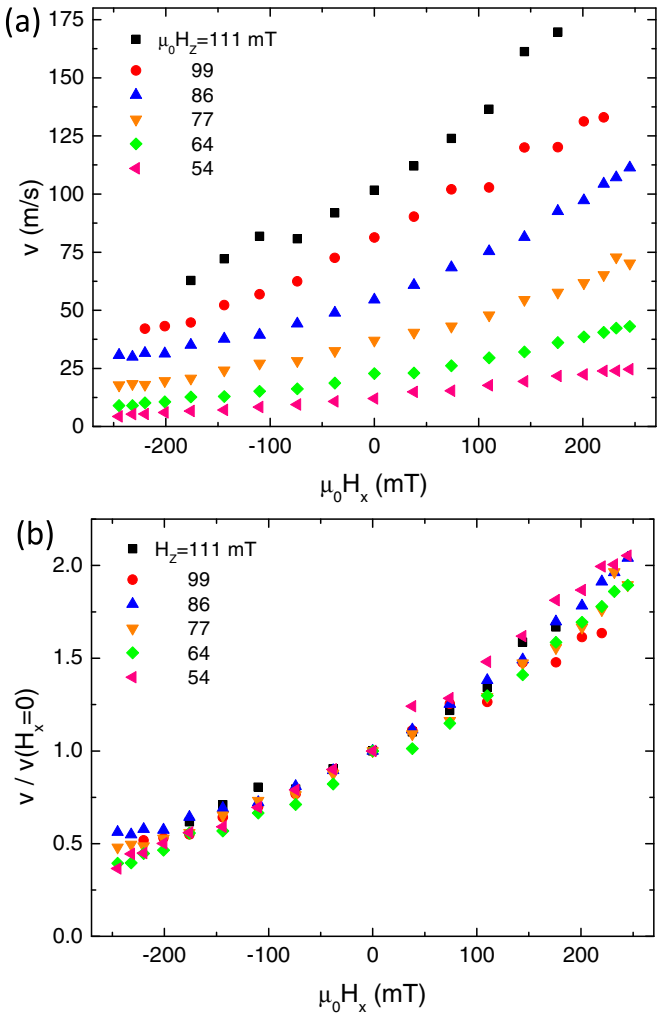

FIG. 4. (a) Averaged DW velocity as a function of the x field for constant values of the z field. (b) Averaged DW velocity normalized by DW velocity in the absence of the x field.

Figure 4(a) shows that the modulation of DW velocity is affected similarly by H_x regardless of the value of H_z. This statement is confirmed by the superposition of all the curves when normalized by the DW velocity in the absence of the x field [Fig. 4(b)]. Note that, although the qualitative behavior reported in Figs. 3(c) and 4 is identical, the velocity values are different for the same field H_z. This can be explained by a slight difference of magnetic properties for the two samples or/and by a small variation of the magnetic field H_z due to the repositioning of the microcoil on the new sample. The data of Fig. 4 are finally plotted as DW velocity versus H_z for different H_x values (Fig. 5). These data show that H_x affects continuously the DW mobility by accelerating or slowing down the DW depending on the H_x direction. We note again that no discontinuity corresponding to the Walker breakdown appears, regardless of the sign and the magnitude of H_x, over the range of fields studied. Finally, we remark that no DW tilts were observed after the field pulses [those seen for a few initial DW positions in Fig. 3(b) correspond to two defects close to the center of the stripe]. One may first think that the sample quality is such that the DW can fully relax to

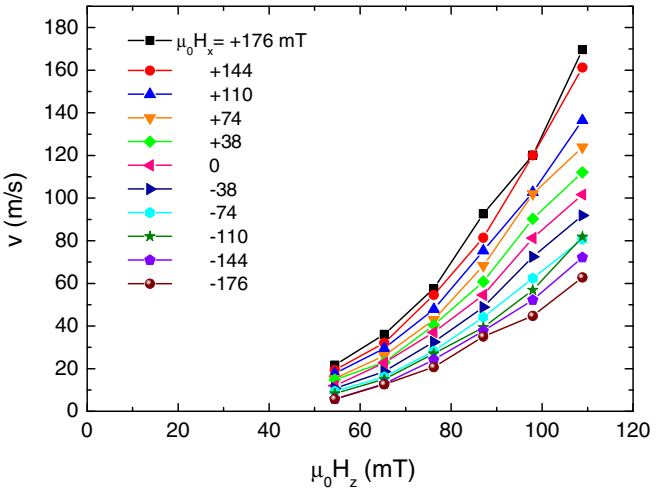

FIG. 5. DW velocity as a function of the z field for constant values of the x field.

the equilibrium zero tilt angle. This view is disproved by the observation of irregular domain wall shapes (see Fig. 1 for magneto-optics, and Ref. [29] for higher-resolution images on the same sample by near-field magnetic microscopy). The alternative explanation is that DWs do not appreciably tilt during their motion.

III. MICROMAGNETIC ANALYSIS

The experimental results shown above are at salient variance with the first theoretical study of the dynamics of Dzyaloshinskii domain walls (DDWs) [10], where the in-plane field was seen to change the Walker breakdown field (in a chiral way), but the DW mobility remained almost the same. However, this first exploratory work was limited to low values of the effective micromagnetic DMI constant. This restriction is lifted here. In addition, 2D micromagnetic simulations are performed in order to take into account all degrees of freedom of the DW, most notably the DW tilt across the strip width, whose relevance was recently revealed [27]. These simulations also allow for the introduction of some disorder into the film so as to mimic real samples that show a nonzero DW propagation field. Thermal fluctuations were included only in some test cases. Indeed, they do not play an important role as short field pulses are applied and the creep regime of DW motion is not investigated. The 2D micromagnetic results are compared to those of much faster 1D micromagnetic simulations [that solve a model in which the whole profile $\vec{m}(x,t)$ is the unknown; see Ref. [10] for details] for a perfect sample. This section, although directly inspired by the experimental part described above, can be read as a stand-alone micromagnetic investigation of DW dynamics in asymmetric ultrathin films under large combined fields.

The 2D simulations were performed with two codes. A homemade code [30], modified to include the DMI of interfacial type, was ported to graphical processing units (GPUs, we used NVIDIA's Tesla M2090). Double precision was used throughout, and, as a pseudo-random-number generator, the GPU-specific version of the "Mersenne twister" [31] was used. As this code evaluates the micromagnetic effective field at the

mesh points (centers of the cells), modified micromagnetic boundary conditions [32] have to be introduced in order to compute this field for the nearest and next-nearest points from a boundary. The mesh cells were $a \times a \times 0.6$ nm^3 in size, with $a < 1.5$ nm, which is well below the DW width so as to avoid numerical artifacts, and of the order of the sample thickness for the accuracy of the magnetostatics calculations [30]. In addition, the public code MUMAX3 [33,34] was employed for the largest sizes on single-precision GPUs, thus optimizing calculation speed, using mesh sizes $a = 1$ to 2 nm. The reference frame has x along the length and y along the width of the nanostrip, z being normal to the film. The micromagnetic parameters taken as appropriate for the samples of the experiments are as follows [21,27]: spontaneous magnetization $M_s = 1090$ kA/m, perpendicular uniaxial anisotropy $K_u = 1.25 \times 10^6$ J/m^3, exchange constant $A = 10$ pJ/m, damping constant $\alpha = 0.5$, and gyromagnetic factor $g = 2$. As the samples are much thinner than the DW width or the exchange length, it is meaningful to consider the effective uniaxial anisotropy $K_{\rm eff} = K_u - \mu_0 M_s^2/2$. Derived micromagnetic quantities are as follows: effective anisotropy field $\mu_0 H_{K,\rm eff} = 924$ mT, DW width parameter at rest $\Delta_0 = \sqrt{A/K_{\rm eff}} = 4.46$ nm, and threshold DMI for instability of the uniformly magnetized state $D_{c0} = 4\sqrt{AK_{\rm eff}}/\pi = 2.86$ mJ/m^2. For the DMI, we investigated values of D between 0 and -2.8 mJ/m^2, well above the threshold for the Bloch to Néel wall transition (0.1 mJ/m^2). These are effective values, i.e., DMI is treated as a volume term, as justified by the small thickness of the sample. The negative sign for D corresponds to a CCW (also called left-handed) rotation of moments across the DW [35], as evidenced by these and other experiments [5,8,36,37]. Nanostrips of width $w = 100$ to 2000 nm were investigated, with 1000 nm length (2000 nm for the largest w). Such short lengths could be used because of the "moving calculation box" technique [38]. Disorder was implemented by first distributing the value of K_u for each cell with a Gaussian law having a standard deviation of σ% of the average value given above, and then filtering spatially these anisotropy values by Gaussian convolution with a standard deviation ρ. A disorder profile was created for a very long nanostrip, and the calculation box was moved along this nanostrip during the simulations according to the DW position. When necessary, calculations were repeated under identical conditions, only changing the disorder pattern.

The DW velocity under a sole easy axis (z) field is first investigated in a $w = 100$ nm wide strip. This is already no longer a 1D situation, as the strip width is well above the size of a 2π Bloch line. The latter, in the limit where DMI dominates over DW demagnetizing energy, is indeed analytically given by $2\pi\sqrt{A\Delta_0/(\pi|D|)}$ (24 nm for $D = 1$ mJ/m^2). Results for a medium DMI $D = -0.6$ mJ/m^2 are shown in Fig. 6(a). In this calculation, field is applied at time $t = 0$ and kept constant, and the DW position is monitored for 25 ns. Without disorder, velocity is linear in field up to the Walker field ($\mu_0 H_z = 99$ mT, much above the value of 9 mT computed for zero DMI). Above this field, velocity falls to a lower value, with a disappearance of the negative mobility regime, this regime (dashed curve) being characteristic of 1D dynamics [22]. When disorder is present and the field is large (above 75 mT here), the DW is never blocked, but the average velocity (over 16 trials) is reduced markedly, especially below the Walker field (see

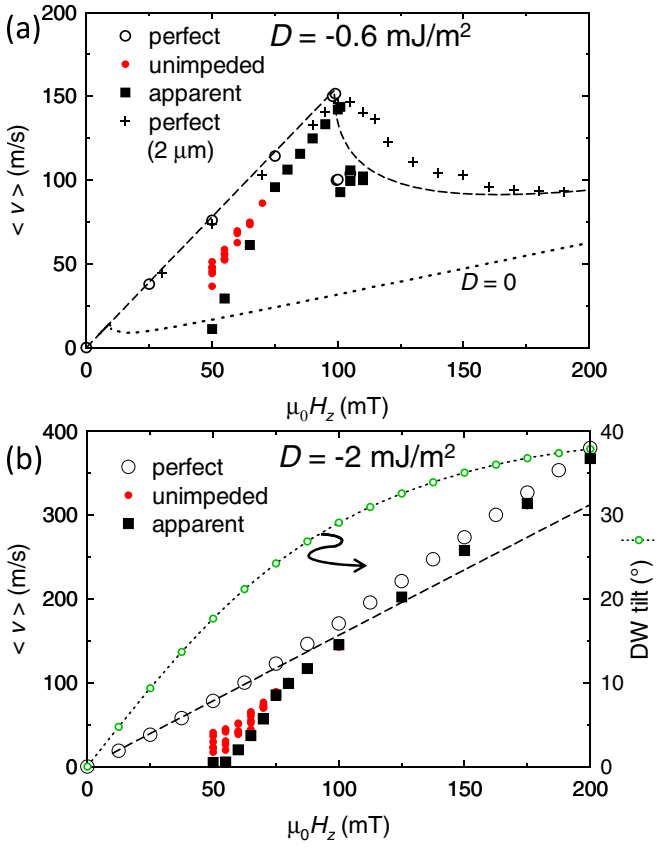

FIG. 6. Computed long-time average domain wall velocity under an easy-axis field in a nanostrip 100 nm wide (2D simulations), with $D = -0.6$ (a) and -2 mJ/m^2 (b). Open symbols are for the perfect sample and full symbols for imperfect ones, the small circles showing the unimpeded velocity (for different realizations of disorder) and the squares the apparent velocity. Note the increase of velocity in the case $D = -2$ mJ/m^2 due to the tilt of the domain wall (right-hand scale) and the different velocity scales for (a) and (b). Crosses in (a) show the result for a perfect sample 2 μm wide.

Appendix A for an analytical model of this reduction). For lower fields, the DW may stop for some time or until the end of the simulation. In such a case, we first define an apparent velocity (full squares) as the final DW displacement divided by the simulation duration, similar to experiments in which field pulses are applied and only the final DW position is measured. In addition, we compute an "unimpeded" velocity by dividing the final displacements by the elapsed time up to the blocking of the DW. The apparent average velocity is close to 0 at about 50 mT, similar to experiments. As shown in other simulation studies [39], the effect of thermal fluctuations is mainly to reduce the time when the DW is blocked, thus moving the apparent velocity up toward the unimpeded value. Hence, nonzero velocities at low fields ($\mu_0 H_z < 50$ mT) are anticipated, located in-between the unimpeded and apparent values, depending on pulse duration and nanostrip width. The typical disorder strength was determined by these calculations: $\rho = 1.5$ nm, $\sigma = 15\%$ for small w, and 22% for the largest w. Note that this value for the Gaussian filtering length ρ gives patches extending over 5 nm, comparable to the grain size and to the DW width. For a larger D value [for example

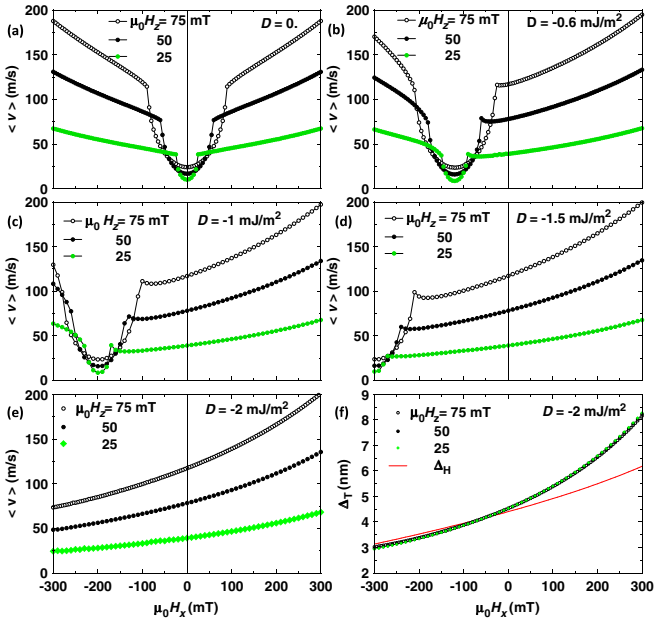

FIG. 7. Computed (one-dimensional micromagnetics) domain wall velocity variation under an in-plane field transverse to the DW, for $D = 0$ (a), -0.6 (b), -1.0 (c), -1.5 (d), and -2 mJ/m^2 (e). The DW is driven by three values of H_z, and a positive H_x favors its in-plane magnetization. In the precessional regime, the time average of the velocity is shown. Panel (f) shows the computed Thiele DW widths in the case $D = -2$ mJ/m^2 for the same values of the z field, as well as the "imaging" Hubert DW width Δ_H.

$D = -2$ mJ/m^2, Fig. 6(b)], the DW velocity computed with 2D micromagnetics is larger than for 1D micromagnetics, as the DW tilts [27] [Fig. 6(b), right-hand scale]. The limiting D value for which DW tilt effects become important can be estimated from the extended collective coordinates model including DW tilt [27], with the result that it is $D_{c0}/2$ typically [40]. In addition, as DMI is more than three times larger than the previous case, Walker breakdown is not seen in the investigated field range. These results are not specific to the $w = 100$ nm strip width, as similar results were obtained for $w = 2$ μm, except for the negative mobility region [Fig. 6(a)]. Thus, compared to 1D modeling of a perfect sample, the steady-state regime sees its velocity increased by DW tilting but decreased by disorder.

An in-plane field H_x applied normal to the DW stabilizes or destabilizes its structure according to its sign relative to the sign of the DMI. The effect of such a field on the DW velocity, for different values of the z field and for several values of the DMI, is illustrated in Fig. 7. These curves, obtained by 1D micromagnetic simulations for perfect samples, use the same reference situation of a down/up DW driven by a negative H_z and stabilized by a positive H_x. The average velocity over long times is evaluated here. The curves consist of two parts. At large in-plane fields (both signs), the DW structure is stable and DW motion takes place in steady-state conditions, with a large velocity. For the fields in between, the DW moment precesses and the DW velocity is strongly reduced (Walker breakdown). For $D = 0$ [Fig. 7(a)], the velocity increase at large x fields is symmetric, as the DW structure is of the Bloch type at $H_x = 0$. This increase is due to the increase of the Thiele width [41,42] of the DW. As D becomes larger, the velocity versus in-plane field curve becomes increasingly asymmetric [Figs. 7(b) and 7(e)], as, in the first approximation, DMI acts on the DW as a chiral in-plane field transverse to the DW. One notices that the Walker breakdown region appears to undergo a rigid translation along the H_x axis as D varies, in agreement with the concept that DMI creates a chiral in-plane field within the DW. Hence, the bottom velocity at the center of the Walker breakdown region is the same as the precessional velocity under the same H_z and $D = 0$ [plotted in Fig. 6(a)]. For $|D| > 2$ mJ/m^2, the Walker breakdown has completely disappeared from the investigated window in the x and z fields. In the case in which DMI dominates the DW demagnetizing energy, the two fields limiting the breakdown region are simply expressed in the collective coordinates model [4,10] by

$$H_x = \frac{D}{\mu_0 M_s \Delta} \pm \frac{2}{\pi}\frac{H_z}{\alpha}, \tag{2}$$

with good accuracy. For example, -26 and -217 mT are obtained for $D = -0.6$ mJ/m^2 and $\mu_0 H_z = 75$ mT when using the zero-field DW width Δ_0. See Appendix B for the justification of using Δ_0, the DW width parameter at rest, in Eq. (2).

We note that, for the large value of D [Fig. 7(e)], the calculations agree qualitatively with the experimental results shown above. In that case, the computed Thiele DW widths [Fig. 7(f)] increase with the x field independently of the z field value. The values are very close to the analytical calculation (see Appendix B). Note that, in the presence of an in-plane field, the stationary mobility is modified to $v/H = (\gamma_0/\alpha)\Delta_T m_{z0}$, where $m_{z0} = \sqrt{1-(H_x/H_{K,\mathrm{eff}})^2}$ is the reduced easy-axis magnetization in the domains, so that the velocity increase due to the increase of the Thiele DW width is partly compensated by the effect of magnetization rotation in the domains. Therefore, the Thiele DW width alone does not fix the DW velocity. For the calculations performed here, however, m_{z0} reached only 0.95 at the largest x fields, so that the normalized velocity curves do correspond to the variation of the Thiele DW width. When looking at these results, one should not forget that the Thiele DW width is not a geometrical width, e.g., to be measured by imaging, but a quantity linked to the energy dissipation at the moving DW. To illustrate this point, the "imaging" DW width introduced by Hubert [43] is also plotted in Fig. 7(f) [the data being also very close to the analytical value (Appendix B)].

These one-dimensional micromagnetic simulations are, however, too simple, as they do not address the influence of the finite width of the samples as well as the effects of disorder [see Fig. 6(b)]. With 2D simulations and for $w = 100$ nm, the effect of the in-plane field on the DW velocity (long time average) under a fixed $\mu_0 H_z = 75$ mT is shown in Fig. 8. For a medium DMI value [-0.6 mJ/m^2, $|D|/D_{c0} = 0.21$, Fig. 8(a)], the DW tilting (change of DW x position as a function of the y position) is minor as the DW energy is still large [27]. Thus, only the effect of disorder is seen, with a velocity reduction in the steady-state regime and a tiny change of velocity in the

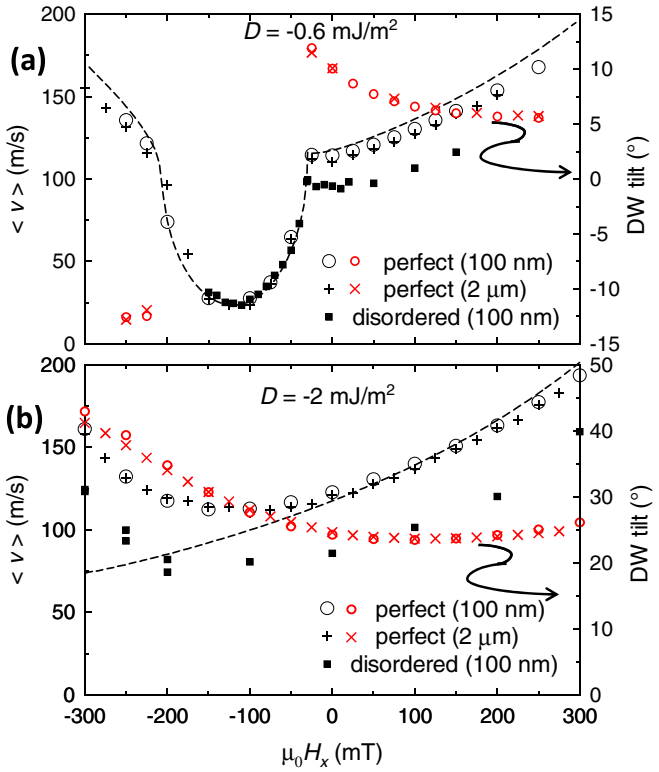

FIG. 8. Computed (two-dimensional micromagnetics, stripe width 100 nm, drive field $\mu_0 H_z = 75$ mT) domain wall long-time average velocity variation under an in-plane field transverse to the DW, for $D = -0.6$ mJ/m^2 (a) and $D = -2$ mJ/m^2 (b). Results for a perfect and a disordered nanostrip are shown (open and full symbols, respectively), and the values of the steady-state DW tilt angle are plotted for the perfect sample (right scale). The dashed curves show for comparison the 1D micromagnetics results for the velocity, and the crosses are the 2D micromagnetic results for a perfect sample of 2 μm stripe width.

precessional regime, as already seen in Fig. 6(a) in the absence of an in-plane field.

In contrast, for a larger DMI value [-2 mJ/m^2, $|D|/D_{c0} = 0.7$, Fig. 8(b)] where the precessional regime is not reached in the investigated x field range, the tilt strongly affects the dependence of velocity on an in-plane field, as best seen in the results for the perfect sample. Note that the change of velocity at negative x fields between 1D and 2D micromagnetics is larger than the simple $1/\cos\chi$ effect (with χ the DW tilt angle [27]), because the whole DW structure (for example, its Thiele width) is changed when it tilts, as the in-plane field is fixed. For an even larger value of D (-2.4 mJ/m^2, not shown), the velocity increase at large negative fields is less important but still noticeable, as the Walker breakdown region is farther from the investigated field range. Again, we note that the strip width does not play a big role, as simulations with $w = 2$ μm (Fig. 8, crosses) produce results that are extremely close to those at $w = 100$ nm, even in the Walker breakdown regime of Fig. 8(a). This nonmonotonous variation of velocity versus in-plane field, not suppressed by disorder, is in strong opposition with the experimental results.

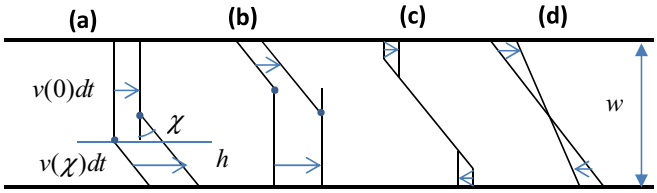

FIG. 9. Sketch of the DW tilt buildup and relaxation. In (a) and (b), the DW, initially vertical, is driven by a force. A tilted segment (with the steady-state tilt angle χ) develops from the bottom edge of the nanostrip and propagates linearly to the upper edge, at a time T_{d2} (a). If the tilted segment moves more slowly than the vertical one, the tilt builds up from the upper edge (b). The relaxation can occur in the two-slope (c) or one-slope (d) modes. In the former case, the DW end points on the edge move toward the center as the square root of time, removing the tilt at a time T_{r2}. In the latter case, tilt relaxes exponentially with a time constant τ_{r1}.

It was shown in a previous publication [27] that the DW tilt along the y direction is a slow variable, having a relaxation time that increases—in a first approximation—as the square of the nanostrip width. As the experiments were performed with 20-ns-long z field pulses on $w = 2$ μm strips, this duration should be compared with the tilt characteristic time. In a first step, the dynamics of the DW tilt was studied by simulations for perfect nanostrips of various widths w. These reveal different processes by which the DW tilt changes.

When the wall is driven toward a steady-state motion, we know from the previous part that a steady-state tilt angle χ exists, with an associated DW velocity along the strip denoted by $v(\chi)$. When starting from the zero-field equilibrium where $\chi = 0$, the DW initially moves with the velocity found in the one-dimensional simulations shown above, called $v(0)$. One process by which the tilt angle changes from 0 to χ, called the two-slope mode, is sketched in Fig. 9(a). It is more and more clearly observed as the strip width becomes larger. In this process, the tilt builds up from one side of the nanostrip [determined by the signs of the steady-state tilt and of the velocity difference $v(\chi) - v(0)$]. A simple geometric calculation shows that the breakpoint height h between the two slopes moves in the y direction according to $dh/dt = [v(\chi) - v(0)]/\tan\chi$. As shown in Figs. 9(a) and 9(b), the argument does not depend on the fact that $v(\chi)$ is larger or smaller than $v(0)$, as only the edge where the tilted segment appears is changed. Thus, after a time

$$T_{d2} = \frac{w \tan\chi}{|v(\chi) - v(0)|}, \tag{3}$$

the DW is tilted to the steady value. This model is easily generalized to a nonzero initial tilt angle. It is important to realize that T_{d2} is not a fixed time constant: if, for example, the driving force is a z field, reducing it decreases both the velocities as well as the steady-state value of χ. Another important feature is that this time depends linearly on the strip width w.

After suppression of the external driving force, only the gain of DW energy by going back to $\chi = 0$ is acting on the wall (we forget here the automotion effect linked to the relaxation of the DW magnetization [44], as the DW width is small in the samples considered). In the two-slope mode, starting from a

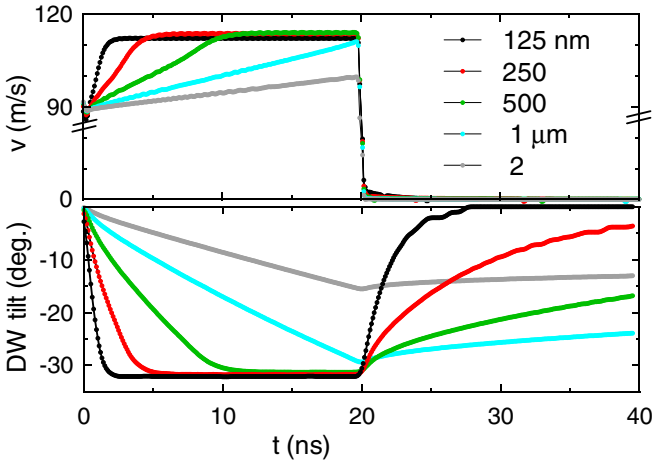

FIG. 10. Plot of the DW velocity and DW tilt vs time, for $D = 2$ mJ/m^2, $\mu_0 H_x = -150$ mT, and $\mu_0 H_z = 75$ mT applied at time $t = 0$ for 20 ns, as computed for perfect nanostrips by 2D micromagnetic simulations. Different widths of the nanostrip are shown, between 100 nm and 2 μm. Note the break on the velocity axis.

uniformly tilted wall at angle χ, one finds that the end point of the wall at the nanostrip edge [Fig. 9(c)] relaxes as the square root of time, reaching equilibrium at time

$$T_{r2} = \frac{w^2 \alpha \mu_0 M_s}{2\gamma_0 \Delta\sigma} \frac{\cos^2(\chi/2)}{\cos\chi}. \quad (4)$$

This formula is very close to that [27] giving the time constant τ_{r1} of the tilt relaxation in the one-slope model [Fig. 9(d)], as in the vicinity of $\chi = 0$ the latter simply substitutes a factor $1/3$ into the χ-dependent fraction in Eq. (4). Thus, whether by a one-slope or by a two-slope mode, the tilt relaxation requires times that scale as the square of the strip width. Simulations also show that the two relaxation modes may occur simultaneously. However, this does not change the tilt relaxation time significantly. These different processes are illustrated in Fig. 10, where the time evolution of DW velocity and tilt is plotted as a function of the nanostrip width w. When field is applied, velocity changes quasilinearly between $v(0)$ (reached very rapidly as this involves only a rotation of the DW magnetization) and $v(\chi)$, mirroring the quasilinear evolution of the tilt angle from 0 to χ. One sees that, for the representative values of the x and z field that are applied, tilt does not reach its steady-state value at the end of the 20 ns pulse, as soon as $w > 1$ μm [the values extracted for T_{d2} agree with Eq. (3) for the larger widths]. Thus, the effective velocity defined as the total DW displacement divided by the 20 ns pulse time decreases to $v(0)$ as the strip width increases, so that for the 2 μm sample the velocity increase due to the DW tilt becomes quenched. When the field is cut, the velocity falls very rapidly to zero, whereas the tilt relaxes on a time scale that indeed increases even faster than w^2 (the fitted times for zero tilt T_{r2} are 470 ns for $w = 1$ μm and 90 ns for 500 nm, for example). The conclusion of this study on perfect samples is that, when the pulse is much shorter than the time to buildup the steady-state tilt, the 2D modification of the DW velocity through the tilt is strongly reduced.

IV. DISCUSSION

The goal of this paper is to discuss the physics of DW motion in asymmetric ultrathin films, triggered by the experimental results shown in Sec. II. Thus, we have not explored by systematic simulations the range of micromagnetic parameters that would best reproduce the sample behavior, given that some of them are hard to determine directly (notably, the exchange constant). Nevertheless, as we took accepted values for the micromagnetic parameters of the sample, we now compare the sets of results from experiments and calculations.

Looking first at the velocity to z field relation (Fig. 2 versus Fig. 6), one sees that the inclusion of DMI provides a natural explanation to the large velocities that are measured, with no sign of Walker breakdown, as remarked earlier [10]. From analytical results [10] and as confirmed by 1D micromagnetic simulations, it is possible to see that $|D| > 0.8$ mJ/m^2 is required to reproduce the absence of breakdown in these conditions. Calculations performed in the presence of disorder and at the full nanostrip width confirm this conclusion, as breakdown is not suppressed by disorder, even for the large 2 μm nanostrip width (not shown).

Considering now the effect of the additional in-plane field normal to the DW (Fig. 4 versus Fig. 7), we observe that the micromagnetic 1D model reproduces qualitatively the experiments when considering a large DMI (larger than 1.5 mJ/m^2 in absolute value). The factor 4 between the lowest and highest velocities when H_x is varied [Fig. 4(b)] is, however, larger than the factor $\approx$2 obtained in 1D micromagnetics for a perfect sample [Fig. 7(c)]. When taking into account 2D effects, the monotonous variation of velocity with the x field is lost due to the tilt of the DW across the width of the strip (Fig. 8). For larger values of D, the effect is only slightly reduced. Rather, the key point is that these 2D calculations investigate the steady-state, or long-term, DW motion, in which the DW tilt has time to fully develop.

The micromagnetic investigations of the DW motion under 20-ns-long z field pulses for the 2-μm-wide perfect sample (Fig. 10), combined with the calculated values of the velocities $v(\chi)$ and $v(0)$ [Fig. 8(b)], show that, except for the most negative x fields and large z fields, the tilt buildup time T_{d2} is above the pulse duration, so that the apparent DW velocity decreases toward the 1D value. In the presence of disorder, as the applied z fields are not much larger than the DW depinning field, the velocities are smaller than for the perfect sample. On the other hand, the induced DW tilts are nearly unchanged, which can be understood from the fact that the tilt is linked to the orientation of the DW magnetization. Hence, from Eq. (3), longer tilt buildup times are expected under disorder, reinforcing the quenching of the tilt. This is illustrated by the apparent velocities computed under disorder, after one 20 ns z field pulse, for two representative values $\mu_0 H_z = 75$ and 110 mT (Fig. 11). One sees that the experimental behavior of velocity versus in-plane field is reproduced for $|D| \approx 2.2$ mJ/m^2. Indeed, for lower values of $|D|$, the Walker breakdown occurs at the most negative x fields. On the other hand, for larger values, the DW is pinned at many points, resulting in the formation of many filaments [two filaments can be seen in the first image of Fig. 11(b)], announcing the DW instability at $D = D_{c0} = -2.86$ mJ/m^2.

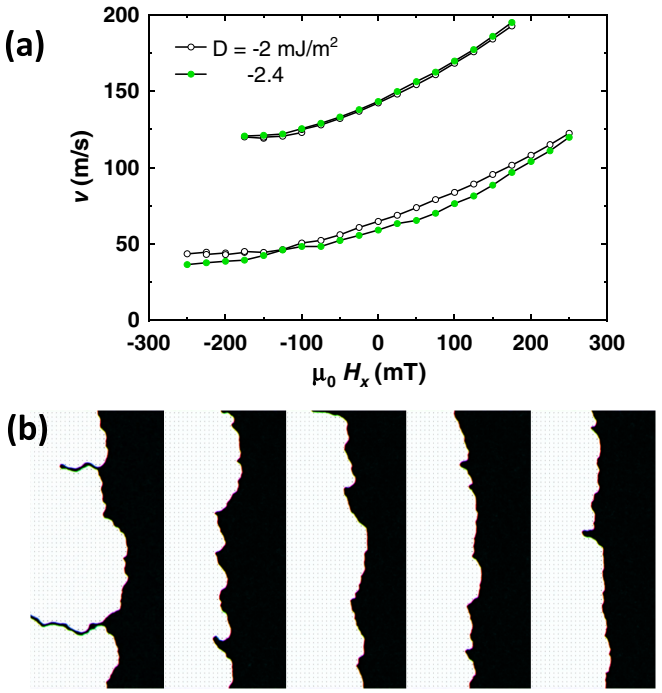

FIG. 11. (a) Computed apparent velocity for the 2-μm-wide strip, with disorder, after applying a single 20-ns-long z field pulse (upper curves: $\mu_0 H_z = 110$ mT, lower curves: 75 mT), as a function of the static x field, for two values of D. (b) DW images after pulse termination ($D = -2$ mJ/m^2, $\mu_0 H_z = 75$ mT, and $\mu_0 H_x = -150$ mT) for five realizations of the disorder.

The computed DW tilts at the end of one pulse are not exactly zero, as shown in Fig. 11(b), but are strongly reduced (from 30 to $5 \pm 5^\circ$ for the case shown), with a spatial standard deviation of the order of the mean value. From the preceding results, one can expect that, with a better model of imperfections that would decrease the calculated velocities down to the experimental values [compare Fig. 11(a) and Fig. 4(a)], these tilts should become even closer to zero. Thus, despite the very long tilt relaxation times, tilt should not accumulate as pulses are repeated. This seems to explain that experimental DW images after the trains of pulses show no systematic tilts.

Summarizing, we conclude that the dynamics of Dzyaloshinskii domain walls is strongly influenced by an in-plane field, especially when DMI is large so that the DW can keep its structure despite large opposite fields. The consequence is a big modulation of easy-axis field-driven velocity, related to a large change of the Thiele DW width. In this dynamics, the tilt of the DW can play an important role, with an impact larger than the $1/\cos\chi$ law, since upon DW tilt the relative orientation of the in-plane field changes. We have shown that the tilt has characteristic times that differ depending on the fact that the wall is driven into a finite velocity state, or just relaxes, the corresponding times scaling as the strip width w or its square, respectively. As a consequence, even for $w = 2$ μm, we find that for relatively short z field pulses (20 ns) the tilt is quenched, so that the 1D micromagnetic simulations are relevant.

This physics was shown to (quasi) quantitatively describe the dynamics of DW in a typical ultrathin Pt/Co/AlOx sample under easy-axis and hard-axis fields. From the ranges of applied fields where no sign of Walker breakdown is observed, and the measured evolution of velocity under an in-plane field, we infer a relatively large DMI ($|D| = 2.2 \pm 0.3$ mJ/m^2 typically, i.e., $|D| \approx 0.8 \times D_{c0}$) in this sample. For a precise value for D, an independent determination of all other micromagnetic parameters is required, together with extensive simulations, but this is beyond the scope of this paper. This work points to the Pt/Co/AlOx samples as candidates for large values of the DMI, and it supports previous conclusions drawn from domain nucleation measurements [8], or combined in-plane field and current-induced DW motion on equivalent or similar samples [5,36,37,45]. The obtained value of DMI also agrees with the first "*ab initio*" calculations of DMI at the Pt(111)/Co interface [46,47], and with more direct measurements of D by Brillouin light scattering [48].

ACKNOWLEDGMENT

This work was supported by the Agence Nationale de la Recherche, Project No. ANR 11 BS10 008 ESPERADO.

APPENDIX A: 1D DOMAIN WALL MOTION IN A RANDOM POTENTIAL

We consider a DW energy that varies with DW position q as $U\cos(kq)$, where k is the wave vector of this nonuniformity. Thus, when driving the DW by an easy-axis field H, the total field acting on the DW depends on position according to $H + h\sin(kq)$ with $h = Uk/(2M_s)$. For a long-wavelength nonuniformity ($k\Delta \ll 1$) and a field lower than the Walker field, the DW position versus time obeys

$$\frac{dq}{H + h\sin(kq)} = \frac{\gamma_0 \Delta}{\alpha} dt. \tag{A1}$$

The integral is analytic, and one finds an average velocity

$$\langle v \rangle = \frac{\gamma_0 \Delta}{\alpha} \sqrt{H^2 - h^2} \tag{A2}$$

(for $|H| < |h|$, the DW is blocked indefinitely at some point so that $\langle v \rangle = 0$). Note that, even if the *space* average of the velocity is unaffected by the nonuniformity, the measurements correspond to the *time* average, resulting in a reduced velocity. To describe a more realistic sample, we consider that it is divided into regions of equal length where h takes different values, with a probability distribution $p(h)$. Computing the time that the DW will need to cross a long distance (containing a large number of regions), the average velocity reads

$$\frac{1}{\langle v \rangle} = \frac{\alpha}{\gamma_0 \Delta} \int \frac{p(h)}{\sqrt{H^2 - h^2}} dh. \tag{A3}$$

This formula is valid for $|H| > |h|$: the distribution of h must be of finite width in this zero-temperature 1D model. From Eq. (A3), $\langle v \rangle$ can be evaluated for simple probability distributions. We consider in the text a triangular law where

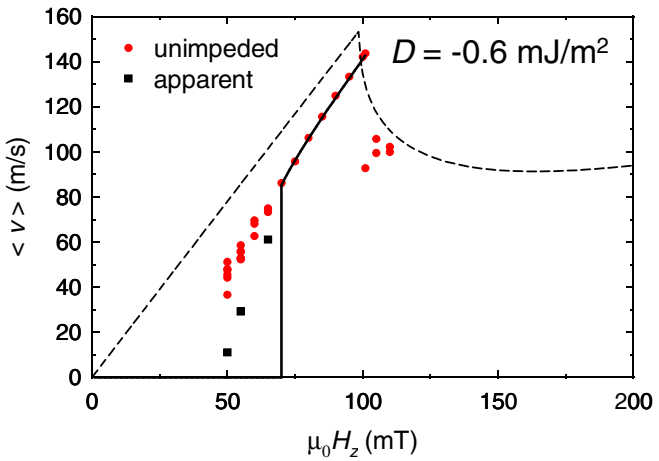

FIG. 12. Computed long-time average domain wall velocity under an easy-axis field in a nanostrip 100 nm wide (2D simulations), with $D = -0.6$ mJ/m^2. Open symbols are for the perfect sample and full symbols for imperfect ones, the small circles showing the unimpeded velocity (for different realizations of disorder) and the squares the apparent velocity. The dashed line is the 1D micromagnetic calculation result, and the line is the analytical model discussed in Appendix B.

$h_{\min} < h < h_{\max}$. The result is

$$\langle v \rangle = \frac{\gamma_0 \Delta}{\alpha} \frac{[(h_{\max} - h_{\min})/2]^2}{f(h_{\max}) + f(h_{\min}) - 2f(h_c)}, \tag{A4}$$

where $h_c = (h_{\min} + h_{\max})/2$ and the auxiliary function reads $f(h) = \sqrt{H^2 - h^2} + h \arcsin(h/H)$.

As an example of application of this model, Fig. 12 shows the calculated DW velocities for a rough strip 100 nm wide with $D = -0.6$ mJ/m^2 as a function of z field, compared to Eq. (A4) with $\mu_0 H_{\min} = 0$ and $\mu_0 H_{\max} = 70$ mT. The latter value was fixed by the field value below which DW stops are calculated. Very good agreement of this simple model to the calculation results is observed.

APPENDIX B: DOMAIN WALL PROFILE AND WIDTHS UNDER AN IN-PLANE FIELD

We extend the 1D calculation of the structure of the Bloch wall under an in-plane field parallel to the wall [49] to the case with interfacial-type DMI and field parallel to the DW magnetization. We consider the ultrathin film situation in which the demagnetizing field can be approximated by $(0,0,-M_s m_z)$: the out-of-plane component is purely local and the in-plane component is neglected. Both approximations rest on the ultrathin film hypothesis that the sample thickness is much smaller than the DW width, and the latter applies well when DMI energy is much bigger than the demagnetizing energy of the Néel wall [10]. As all energy terms favor magnetization in the (x,z) plane, it can be described by a single angle θ with respect to the easy axis, a function of the normal coordinate x. If $h = H_x/H_{K,\text{eff}}$ is the reduced applied field, and $\Delta_0 = \sqrt{A/K_{\text{eff}}}$ is the zero-field DW width parameter, the angle θ satisfies

$$\frac{d\theta}{\sin\theta - h} = \frac{dx}{\Delta_0}, \tag{B1}$$

independently of the value of D. From this profile, the Thiele DW width [41,50] is readily evaluated,

$$\Delta_T = \frac{\Delta_0}{\sqrt{1-h^2} - h \arccos(h)}, \tag{B2}$$

where $h > 0$ means that the applied field is parallel to the DMI effective field in the DW.

To get a more geometrical idea of the DW size, we also compute the DW width introduced by Hubert [43], which applies to any DW. First, the scalar magnetization component m' that changes across the DW has to be determined. If $\vec{m}_1$ and $\vec{m}_2$ are the magnetizations in the domains on both sides of the wall, one has simply $m' = \vec{m} \cdot (\vec{m}_1 - \vec{m}_2)/2$. The DW width is then obtained by the tangent to m' at the DW center ($m' = 0$), upon extrapolation to the values of m' in the domains, resulting in the general formula

$$\Delta_H = \frac{(1 - \vec{m}_1 \cdot \vec{m}_2)/2}{|\partial_x m'|_{m'=0}}. \tag{B3}$$

For the case considered, we obtain

$$\Delta_H = \Delta_0 \sqrt{\frac{1+h}{1-h}}. \tag{B4}$$

As shown in Fig. 7(f), the geometrical width is less affected by field than what would be deduced from the dynamical Thiele DW width.

Finally, in the expression of the DMI effective field within a DW, namely $H_{\text{DMI}} = 2D/(\mu_0 M_s \Delta)$, a DW width Δ appears. Which definition of Δ should be considered for this purpose? As the DW effective DMI field is measured experimentally by applying an in-plane field parallel to it, it is appropriate to define H_{DMI} by comparison of the energies of the DW under DMI and under an in-plane field. From the profile of Eq. (B1), one evaluates these two energies as $-2D \arccos(h)$ and $-2\mu_0 M_s H_x \Delta_0 \arccos(h)$, respectively, showing that the width to consider to evaluate the DMI effective field is simply the zero-field width Δ_0, even when field is applied. This result, which is surprising at first glance, arises from the fact that, for $H_x > 0$, the DW is wider but its angular span is smaller, whereas for $H_x < 0$ the DW is narrower but its angular span is bigger. The two effects compensate perfectly in this approximate 1D analytical model of the DW.

[1] I. M. Miron, P.-J. Zermatten, G. Gaudin, S. Auffret, B. Rodmacq, and A. Schuhl, Phys. Rev. Lett. **102**, 137202 (2009).

[2] I. M. Miron, K. Garello, G. Gaudin, P.-J. Zermatten, M. V. Costache, S. Auffret, S. Bandiera, B. Rodmacq, A. Schuhl, and P. Gambardella, Nature (London) **476**, 189 (2011).

[3] L. Liu, C. F. Pai, Y. Li, H. W. Tseng, D. C. Ralph, and R. A. Buhrman, Science **336**, 555 (2012).

[4] S. Emori, U. Bauer, S. M. Ahn, E. Martinez, and G. S. D. Beach, Nat. Mater. **12**, 611 (2013).

[5] K.-S. Ryu, L. Thomas, S.-H. Yang, and S. Parkin, Nat. Nanotech. **8**, 527 (2013).

[6] S.-G. Je, D.-H. Kim, S.-C. Yoo, B.-C. Min, K.-J. Lee, and S.-B. Choe, Phys. Rev. B **88**, 214401 (2013).

[7] A. Hrabec, N. A. Porter, A. Wells, M. J. Benitez, G. Burnell, S. McVitie, D. McGrouther, T. A. Moore, and C. H. Marrows, Phys. Rev. B **90**, 020402(R) (2014).

[8] S. Pizzini, J. Vogel, S. Rohart, L. D. Buda-Prejbeanu, E. Jué, O. Boulle, I. M. Miron, C. K. Safeer, S. Auffret, G. Gaudin, and A. Thiaville, Phys. Rev. Lett. **113**, 047203 (2014).

[9] I. M. Miron, T. Moore, H. Szambolics, L. D. Buda-Prejbeanu, S. Auffret, B. Rodmacq, S. Pizzini, J. Vogel, M. Bonfim, A. Schuhl, and G. Gaudin, Nat. Mater. **10**, 419 (2011).

[10] A. Thiaville, S. Rohart, É. Jué, V. Cros, and A. Fert, Europhys. Lett. **100**, 57002 (2012).

[11] A. Fert, Mater. Sci. Forum **59-60**, 439 (1990).

[12] A. Fert and P. M. Levy, Phys. Rev. Lett. **44**, 1538 (1980).

[13] I. E. Dzialoshinskii, Sov. Phys. JETP **5**, 1259 (1957).

[14] T. Moriya, Phys. Rev. **120**, 91 (1960).

[15] M. Heide, G. Bihlmayer, and S. Blügel, Phys. Rev. B **78**, 140403(R) (2008).

[16] O. J. Lee, L. Q. Liu, C. F. Pai, Y. Li, H. W. Tseng, P. G. Gowtham, J. P. Park, D. C. Ralph, and R. A. Buhrman, Phys. Rev. B **89**, 024418 (2014).

[17] S. Lemerle, J. Ferré, C. Chappert, V. Mathet, T. Giamarchi, and P. Le Doussal, Phys. Rev. Lett. **80**, 849 (1998).

[18] K.-J. Kim, J. Lee, S.-M. Ahn, K.-S. Lee, C.-W. Lee, Y. J. Cho, S. Seo, K.-H. Shin, S.-B. Choe, and H.-W. Lee, Nature (London) **458**, 740 (2009).

[19] K.-W. Moon, D.-H. Kim, S.-C. Yoo, C.-G. Cho, S. Hwang, B. Kahng, B.-C. Min, K.-H. Shin, and S.-B. Choe, Phys. Rev. Lett. **110**, 107203 (2013).

[20] N. L. Schryer and L. R. Walker, J. Appl. Phys. **45**, 5406 (1974).

[21] P. J. Metaxas, J.-P. Jamet, A. Mougin, M. Cormier, J. Ferré, V. Baltz, B. Rodmacq, B. Dieny, and R. L. Stamps, Phys. Rev. Lett. **99**, 217208 (2007).

[22] K. Yamada, J. P. Jamet, Y. Nakatani, A. Mougin, A. Thiaville, T. Ono, and J. Ferré, Appl. Phys. Express **4**, 113001 (2011).

[23] C. Burrowes, N. Vernier, J.-P. Adam, L. Herrera Diez, K. Garcia, I. Barisic, G. Agnus, S. Eimer, J.-V. Kim, T. Devolder, A. Lamperti, R. Mantovan, B. Ockert, E. E. Fullerton, and D. Ravelosona, Appl. Phys. Lett. **103**, 182401 (2013).

[24] The experimental part of this work was presented orally at the First International Workshop on Spin-Orbit Induced Torque (KAUST, Saudi Arabia, Feb., 2013), and part of the theory at the Workshop on Current Induced Magnetisation Dynamics (Leeds, UK, Jan., 2014).

[25] S. Monso, B. Rodmacq, S. Auffret, G. Casali, F. Fettar, B. Gilles, B. Dieny, and P. Boyer, Appl. Phys. Lett. **80**, 4157 (2002).

[26] K.-S. Ryu, L. Thomas, S.-H. Yang, and S. S. P. Parkin, Appl. Phys. Express **5**, 093006 (2012).

[27] O. Boulle, S. Rohart, L. D. Buda-Prejbeanu, E. Jué, I. M. Miron, S. Pizzini, J. Vogel, G. Gaudin, and A. Thiaville, Phys. Rev. Lett. **111**, 217203 (2013).

[28] K. Mackay, M. Bonfim, D. Givord, and A. Fontaine, J. Appl. Phys. **87**, 1996 (2000).

[29] J.-P. Tetienne, T. Hingant, L. Rondin, S. Rohart, A. Thiaville, E. Jué, G. Gaudin, J.-F. Roch, and V. Jacques, J. Appl. Phys. **115**, 17D501 (2014).

[30] J. Miltat and M. J. Donahue, *Handbook of Magnetism and Advanced Magnetic Materials* (Wiley, New York, 2007), pp. 742–764.

[31] M. Saito and M. Matsumoto, ACM Trans. Math. Software **39**, 12 (2013).

[32] S. Rohart and A. Thiaville, Phys. Rev. B **88**, 184422 (2013).

[33] A. Vansteenkiste, J. Leliaert, M. Dvornik, M. Helsen, F. Garcia-Sanchez, and B. Van Wayenberge, AIP Adv. **4**, 107133 (2014).

[34] Available at http://mumax.github.io/pub.

[35] We use the now adopted convention that a positive D gives rise to a clockwise rotation of the moments [32,51], opposite to that of our initial work [10].

[36] J. H. Franken, M. Herps, H. J. M. Swagten, and B. Koopmans, Sci. Rep. **4**, 5248 (2014).

[37] K.-S. Ryu, S.-H. Yang, L. Thomas, and S. S. P. Parkin, Nat. Commun. **5**, 3910 (2014).

[38] Y. Nakatani, A. Thiaville, and J. Miltat, Nat. Mater. **2**, 521 (2003).

[39] E. Martinez, J. Phys.: Condens. Matter **24**, 024206 (2012).

[40] In the stationary case, and supposing that D is much above the Bloch to Néel transition value D_c (an appropriate approximation for films much thinner than the DW width) [10], one finds that $D/D_{c0} > \sin(\chi_{\rm vis})/\sin(\Phi + \chi_{\rm vis})$ is required, with D_{c0} the critical DMI for the stability of uniform magnetization defined above, Φ the angle of DW magnetization with respect to the local Néel orientation, and $\chi_{\rm vis}$ the threshold tilt angle for detecting tilt effects. When transforming between the frames linked to the DW and to the strip, the cosine of the tilt matters [27], so that we take $\chi_{\rm vis} = \pi/6$ [see Fig. 6(b)]. This means that DW dynamics will be affected by tilt for $D > D_{c0}/2$ typically, thus fixing the limit between "large" and "small" D.

[41] A. A. Thiele, J. Appl. Phys. **45**, 377 (1974).

[42] Y. Nakatani, A. Thiaville, and J. Miltat, J. Magn. Magn. Mater. **290-291**, 750 (2005).

[43] A. Hubert, *Theorie der Domänenwände in Geordneten Medien* (in German), edited by J. Ehlers, K. Hepp, and H. Weidenmüller, Lecture Notes in Physics No. 26 (Springer, Berlin, 1974).

[44] J.-Y. Chauleau, R. Weil, A. Thiaville, and J. Miltat, Phys. Rev. B **82**, 214414 (2010).

[45] E. Martinez, S. Emori, and G. S. D. Beach, Appl. Phys. Lett. **103**, 072406 (2013).

[46] F. Freimuth, S. Blügel, and Y. Mokrousov, J. Phys.: Condens. Matter **26**, 104202 (2014).

[47] B. Dupé, M. Hoffmann, C. Paillard, and S. Heinze, Nat. Commun. **5**, 4030 (2014).

[48] M. Belmeguenai, J.-P. Adam, Y. Roussigné, S. Eimer, T. Devolder, J.-V. Kim, S. M. Cherif, A. Stashkevich, and A. Thiaville, Phys. Rev. B **91**, 180405(R) (2015).

[49] J. Kaczér and R. Gemperle, Czech. J. Phys. **11**, 157 (1961).

[50] A. Thiaville and Y. Nakatani, *Spin Dynamics in Confined Magnetic Structures III* (Springer, Berlin, 2006), pp. 161–206.

[51] E. Martinez, S. Emori, N. Perez, L. Torres, and G. S. D. Beach, J. Appl. Phys. **115**, 213909 (2014).